Research on Engineering Structures & Materials

www.jresm.org

Research Group

Research Article

Data-driven prediction of mechanical properties in friction stir processed Al6061-Alumina composite using enhanced machine learning models

Satish Saini[1,a], Neeraj Kumar[*,2,b], Ranjeev Kumar Chopra[3,c], Monika Mehra[2,d], Ravi Kumar[4,e], Sushil Bhardwaj[5,f], Dinesh Kumar[6,g]

[1]*ECE Department, RIMT University, Punjab, India*
[2]*Dept of Information Technology, VPPCOE& VA, Sion, Mumbai, India*
[3]*School of Computing, RIMT University, Punjab, India*
[4]*ECE Department, Chandigarh University, Punjab, India*
[5]*Department of Physics and Electronics, at Hansraj College, University of Delhi, India*
[6]*Mechanical Eng. Dept., Maharishi Markandeshwar (Deemed to be University) Mullana, India*

Article Info

Article History:

Received 07 Sep 2024

Accepted 01 Dec 2024

Keywords:

Friction stir processing;
Al-6061 alloy;
Alumina;
Mechanical properties;
Special relativity search;
Long short-term memory

Abstract

This study explores friction stir processing (FSP) of Al-6061 aluminum alloy reinforced with alumina nanoparticles, analyzing the effects of processing parameters—including transverse speed, rotational speed, and number of passes—on ultimate tensile strength, yield strength, natural frequencies, and damping ratios. Using a CNC milling machine, FSP was conducted at rotational speeds of 900, 1100, 1300, and 1500 rpm, with traverse speeds of 10, 15, and 20 mm/min. An advanced machine learning model, SRS-optimized long short-term memory (LSTME), was utilized to predict the properties of the processed material, achieving high R^2 values of 0.911 for ultimate strength, 0.951 for yield strength, 0.953 for natural frequency, and 0.985 for damping ratio. Key findings indicate that FSP improves damping characteristics and mechanical properties, with maximum damping effectiveness observed at 900 rpm across all passes. Alumina nanoparticles enhanced damping capabilities, while increased rotational speeds promoted grain refinement, resulting in a stronger, more deformation-resistant material. The LSTME model outperformed other machine learning approaches, reaching R^2 values between 0.965 and 0.993 in training and 0.911 to 0.987 in testing. These results demonstrate the efficacy of combining FSP with machine learning to optimize material properties for high-performance applications.

1. Introduction

Drilling The advancement of composite materials has been crucial in enhancing several engineering disciplines because of its distinctive capacity to amalgamate qualities from diverse materials, yielding components that are stronger, lighter, and more resilient. Initially, composites were fundamental amalgamations created to satisfy basic structural requirements [1]. With technological improvements, composites have developed to include various matrix and reinforcing materials, resulting in high-performance composites appropriate for aerospace, automotive, and marine applications [2]. The use of composites has markedly increased, rendering these materials indispensable in sectors that need lightweight and high-strength characteristics [3]. Aluminum-

*Corresponding author: kumar.d041789@gmail.com
[a]orcid.org/0000-0002-9194-3068:[b]orcid.org/0009-0007-5244-4868; [c]orcid.org/0009-0002-2929-4148; [d]orcid.org/0000-0008-4331-5033; [e]orcid.org/0000-0002-9112-3473; [f]orcid.org/0000-0001-5184-3866; [g]orcid.org/0000-0003-1885-2431
DOI: http://dx.doi.org/10.17515/resm2024.438me0907rs

based composites have gained prominence owing to their superior strength-to-weight ratio, corrosion resistance, and thermal characteristics. Al-6061, a widely used aluminum alloy, is recognized for its adaptability in structural applications. Al-6061 composites, when augmented with ceramic particles or fibers, are appropriate for high-stress applications in automotive, aerospace, and industrial equipment, where durability and performance are paramount [4]. Traditional techniques for producing metal matrix composites (MMCs) include casting, powder metallurgy, and extrusion. These technologies are well-established; nonetheless, they often need elevated temperatures, and protracted procedures, and may encounter challenges in attaining uniform reinforcement distribution. Casting is economical and prevalent; yet, it may result in complications with reinforcement distribution owing to density disparities between the matrix and reinforcement phases [5]. To address the constraints of conventional techniques, innovative manufacturing methods, such as Friction Stir Processing (FSP), have been developed. FSP is a solid-state method that improves mechanical qualities by producing a precise microstructure without melting the material. Friction Stir Processing (FSP) enables meticulous regulation of the distribution of reinforcement particles inside the Al-6061 composite matrix [6]. This procedure generates a homogenous composite with superior mechanical characteristics and higher wear resistance by the application of targeted frictional heat and plastic deformation.

The advancement of composite materials has transformed engineering by presenting alternatives to conventional metals and alloys, delivering a distinctive amalgamation of qualities from both the matrix and reinforcement components [7]. Initially, composites were basic amalgamations of materials intended to fulfill certain structural or functional requirements. Technological breakthroughs have led to the evolution of composites, facilitating the creation of high-strength, lightweight, and durable materials [8]. This progress has catalyzed extensive acceptance across sectors, particularly in applications where weight reduction and superior mechanical strength are critical. Composites are used in several sectors, including aircraft, automotive, sports equipment, and medical devices. They are progressively preferred over traditional materials because of their superior mechanical qualities, corrosion resistance, and capacity for customization [9]. These materials are designed to provide superior performance while minimizing component weight, a characteristic that is especially advantageous in transportation sectors focused on fuel economy and emissions reduction. Aluminum composites have established a unique role within metal matrix composites (MMCs). Although MMCs may use diverse matrices such as titanium, magnesium, and copper, aluminum-based composites are mostly favored owing to aluminum's low density, superior corrosion resistance, and advantageous cost-to-performance ratio [10]. Titanium-based composites provide elevated strength and thermal resistance; yet, they are associated with increased prices and density [11]. Magnesium composites have lightweight properties but are deficient in mechanical strength compared to aluminum [12]. Aluminum composites provide a harmonious combination of strength, weight, and cost, making them a flexible option across several sectors. Aluminum composites are extensively used in industries where weight and durability are essential considerations [13]. In the aerospace sector, they are used in structural components such as wings and fuselage sections [14]. Aluminum composites are used in vehicle production for engine components, wheels, and brake systems, enhancing fuel economy and performance [15]. Aluminum composites are advantageous for the maritime and electronics sectors because to their corrosion resistance and thermal stability, rendering them suitable for components subjected to severe conditions or necessitating efficient heat dissipation [16].

Al-6061 is a highly flexible and extensively used aluminum alloy, esteemed for its superior mechanical qualities, weldability, and resistance to corrosion. Al-6061, categorized under the 6xxx family of aluminum alloys, is mostly alloyed with magnesium and silicon, resulting in a distinctive amalgamation of strength, toughness, and favorable machinability. This alloy is used in diverse industrial applications, including aerospace and automotive components, as well as structural elements in construction, owing to its capacity for facile forming, welding, and heat treatment to improve its mechanical characteristics [17]. Al-6061 is used in components such as frames, pipelines, maritime fittings, and recreational equipment, where strength, lightweight properties, and durability are critical [18]. The Al-2024 alloy, belonging to the 2xxx class, is mostly alloyed with copper, imparting it remarkable strength and fatigue resistance [19]. The Al-7075 alloy is recognized for its remarkable strength; it is an aluminum-zinc alloy that almost matches the strength of some steels while being much lighter. Although Al-7075 exhibits worse corrosion resistance compared to Al-6061, it is often used in applications demanding optimal strength with lowest weight [20]. The Al-5052 alloy is part of the 5xxx family, recognized for its superior corrosion resistance, especially in marine settings, attributed to its elevated magnesium concentration [21]. Al-3003, a widely used aluminum alloy, is alloyed with manganese, offering moderate strength and superior corrosion resistance [22]. Al-6063, like to Al-6061, belongs to the 6xxx class but is mostly selected for its enhanced extrudability and visual appeal. It is often used for architectural and decorative purposes, including window frames, door frames, and metal furnishings. Despite possessing inferior strength compared to Al-6061, Al-6063's superior corrosion resistance and exceptional anodizing characteristics make it appropriate for outdoor and ornamental uses. Every aluminum alloy provides a unique equilibrium of characteristics, including strength, corrosion resistance, formability, and machinability, making aluminum alloys essential in contemporary industries. Al-6061 is widely preferred for its varied performance; nevertheless, other alloys such as Al-2024, Al-7075, Al-5052, Al-3003, and Al-6063 are also essential in specific applications within the aerospace, marine, automotive, and architectural industries.

The investigation used a CNC milling machine to examine the influence of processing factors, including feed rate, number of passes, and rotational speed, on critical material characteristics such as ultimate strength, yield strength, natural frequencies, and damping ratios of the samples [23]. These qualities are essential for evaluating material performance in applications necessitating mechanical robustness and dynamic stability. Conventional modeling techniques often fail to accurately represent the intricate, nonlinear relationships among these factors, particularly when forecasting dynamic attributes such as natural frequencies and damping ratios [24]. To address these issues, an advanced machine learning approach called SRS-optimized Long Short-Term Memory with Embedded Learning (LSTME) was used. The SRS-optimized LSTME model is explicitly designed to process sequential data, making it suitable for capturing the complex temporal patterns and relationships intrinsic to CNC milling operations [25]. This method integrates the capabilities of Long Short-Term Memory (LSTM) networks, recognized for their proficiency in managing time-series data, with Special Relativity Search (SRS) optimization. The SRS component emphasizes frequency-domain analysis, enabling the model to enhance its comprehension and prediction of reactions associated with the material's dynamic behavior, including natural frequency and damping ratio. The integrated learning capacity of LSTME allows the model to learn and adapt in real-time with the introduction of new data, hence improving its accuracy and resilience [26]. The implementation of the SRS-optimized LSTME model commences with a training phase, using previous data from CNC milling trials to elucidate the correlations between processing parameters and material attributes. During the SRS optimization phase, the model focuses on the spectral attributes that most profoundly affect dynamic responses. Upon training, the model can precisely forecast ultimate and yield strengths, together with dynamic characteristics such as natural frequencies and damping ratios, derived from fresh CNC milling inputs. The model's performance is meticulously verified against experimental data, using accuracy measures such as mean absolute error (MAE), root mean square error (RMSE), and R-squared (R^2) values to assess its prediction dependability. The benefits of using SRS-optimized LSTME in this setting are substantial [27]. By including both temporal and spectral attributes of the CNC milling process, the model attains superior prediction accuracy and adaptively modifies to fluctuating milling settings, making it more adaptable than conventional machine learning techniques [28]. This methodology enables producers to forecast the mechanical and dynamic characteristics of milled samples, so considerably reducing the need for comprehensive experimental testing, resulting in time and cost savings. Moreover, the model's real-time predictive capabilities allows immediate process modifications, so assuring uniform product quality. In conclusion, SRS-optimized LSTME offers a comprehensive solution for comprehending and refining CNC milling parameters, allowing businesses to attain specified material characteristics and improved process regulation. In this work, Aluminium alloy 6061 (Al-6061) was used as the matrix material for metal matrix composites (MMCs), with alumina (Al_2O_3) serving as the reinforcing component [29]. Al-6061/Alumina MMCs provide an advantageous amalgamation of lightweight, high strength, and wear resistance, rendering them appropriate for diverse applications across various sectors. These composites improve mechanical qualities, including strength, stiffness, wear resistance, and corrosion resistance, which are essential for rigorous operating settings. Furthermore, by adjusting the volume percentage and dimensions of alumina reinforcement particles, the composite's density may be decreased relative to steel, making it an optimal choice for lightweight applications. To enhance these qualities, we used sophisticated machine learning techniques to forecast the optimal processing parameters for Friction Stir Processing (FSP) of Al-6061 alloy augmented with alumina nanoparticles. Our aim was to use machine learning to determine the ideal FSP conditions that improve the mechanical performance and longevity of the composite [30]. This novel methodology offers a data-driven resolution to enhance the efficiency and efficacy of the FSP process, resulting in advanced Al-6061/alumina nanocomposites designed for high-performance applications. During the investigation, we examined the mechanical characteristics and dynamic reactions of the treated materials under different FSP settings. Employing advanced machine learning methods, namely a refined Long Short-Term Memory with Embedded Learning (LSTME) model augmented by Spectral Response Surface (SRS) optimization, we precisely predicted the mechanical properties of the samples. The LSTME-SRS model was meticulously assessed against three other machine-learning algorithms to measure its predicted accuracy and overall performance. This extensive modelling methodology has shown significant promise for improving FSP parameters, hence aiding in the creation of high-performance Al-6061/Alumina MMCs appropriate for lightweight and durable applications. In this work, Aluminum alloy 6061 (Al-6061) was used as the matrix material for metal matrix composites (MMCs), with alumina (Al_2O_3) serving as the reinforcing component [31]. Al-6061/Alumina MMCs provide an advantageous amalgamation of lightweight, high strength, and wear resistance, rendering them appropriate for diverse applications across various sectors. These composites improve mechanical qualities, including strength, stiffness, wear resistance, and corrosion resistance, which are essential for rigorous operating conditions. Furthermore, by adjusting the volume percentage and dimensions of alumina reinforcement particles, the composite's density may be decreased relative to steel, making it an optimal choice for lightweight applications. To enhance these qualities, we used sophisticated machine learning techniques to forecast the optimal processing parameters for Friction Stir Processing (FSP) of Al-6061 alloy augmented with alumina nanoparticles [32]. The aim of the study is to use machine learning to determine the ideal FSP conditions that improve the mechanical performance and longevity of the composite. This novel methodology offers a data-driven resolution to enhance the efficiency and efficacy of the FSP process, resulting in enhanced Al-6061/alumina nanocomposites designed for high-performance applications. During the investigation, we examined the mechanical characteristics and dynamic reactions of the treated materials under several FSP settings. Employing advanced machine learning methods, namely a refined Long Short-Term Memory with Embedded Learning (LSTME) model augmented by Spectral Response Surface (SRS) optimization, we precisely predicted the mechanical properties of the samples. The LSTME-SRS model was meticulously assessed in comparison to three other machine-learning algorithms to determine its predicted accuracy and overall efficacy. This extensive modeling methodology has shown significant promise for improving FSP parameters, hence aiding in the creation of high-performance Al-6061/Alumina MMCs appropriate for lightweight and durable applications.

2. Materials and Method

2.1 Matrix and Reinforcement

The base of the structure was a sheet of Al-6061 aluminum alloy, which had a thickness of 4 mm. The Al_2O_3 nanoparticle was used as reinforcement.

Table 1. Composition of Al-6061 alloy

Elements	Al	Mg	Si	Fe	Cu	Cr	Mn
Wt.%	98.00	0.797	0.51	0.257	0.219	0.157	0.043

Table 1 displays the outcomes of the chemical analysis performed on the aluminum alloy and the FSP tool using a spectroscopic analyzer. The transmission electron microscopy (TEM) analysis revealed that the reinforcing particles exhibited a high level of purity, measuring at 99.9 percent, and had an average size of 16±5.6 nm as shown in Figure 1.

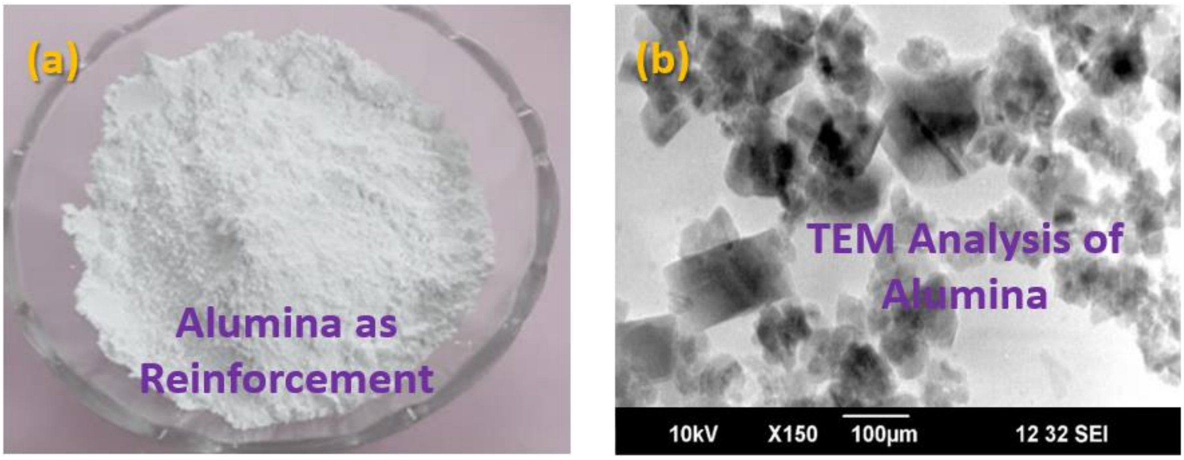

Fig.1. (a) Al_2O_3 powder in typical form and (b) TEM Analysis of Al_2O_3 nanoparticles

2.2 Composite Fabrication Method

Friction Stir Processing (FSP) is a solid-state joining method aimed at improving the microstructure and characteristics of materials, especially metals such as aluminum. The procedure starts with the production of an aluminum sheet, which is precisely machined to form longitudinal grooves that will subsequently contain the reinforcing particles.

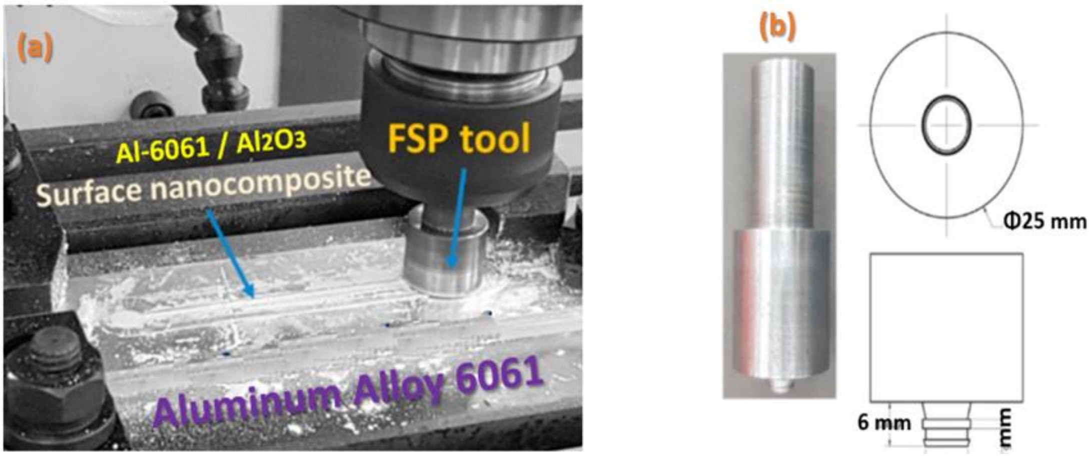

Fig. 2. (a) Tool specifications and (b) FSP processing on Base Alloy

For this particular FSP procedure, a tool with a tapered square form is used to provide excellent contact with the aluminum matrix during processing. A CNC milling machine is configured with the selected tool, which is then brought into contact with the prepared aluminum sheet. The tool rotates at varying rates of 900, 1120, 1400, and 1800 revolutions per minute while traversing the sheet at speeds of 10, 15, and 20 millimeters per minute. The interplay of rotational and translational motion produces frictional heat and mechanical deformation, facilitating the effective alteration of the microstructure in the treated areas. In accordance with the FSP procedure, surface flaws are rectified by grinding with silicon carbide paper, using grit sizes ranging from 450 to 2200. This stage is essential for attaining a polished surface, following which the ground samples are rinsed with water to remove any abrasive residues or metallic particles.

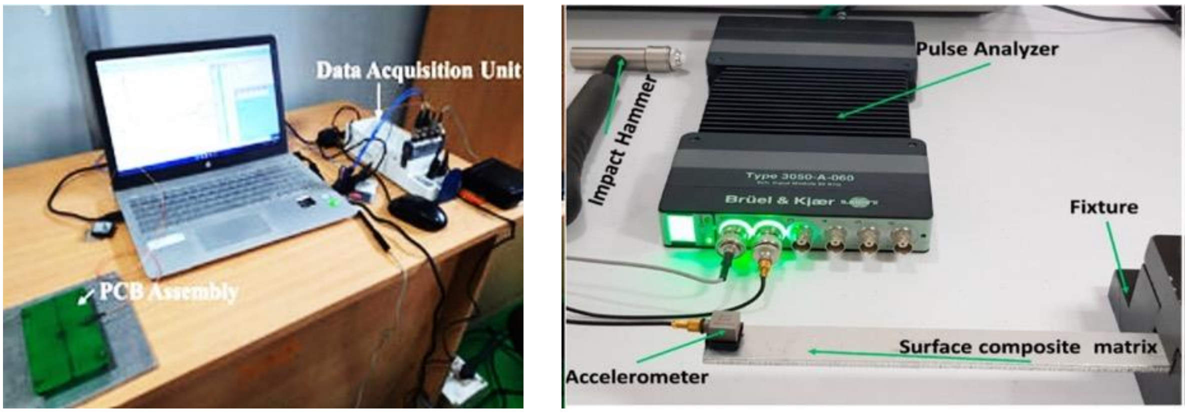

Fig. 3. Free impact vibration 3050 Pulse analyzer

The samples are subjected to an etching process using a solution of hydrofluoric acid, nitric acid, and filtered water at room temperature to improve surface quality and expose microstructural characteristics. The etching procedure is essential for elucidating the microstructure and macrostructure of the treated materials. The samples are examined until the requisite surface quality is achieved, guaranteeing comprehensive cleaning prior to analysis. Flat dog bone-shaped samples are extracted from the middle of the treated zone for mechanical property assessment, in compliance with ASTM requirements. The samples, constructed with precise dimensions, are subjected to tensile testing using a Universal Testing Machine (UTM) with a maximum load capacity of 100 kN, in compliance with ASTM B557 standards. The natural frequency and damping factor of the composite surface are evaluated by free vibration analysis. Accelerometers are affixed to the samples to assess their vibrational response over time, using a pulse data analyzer and an impact hammer. Multiple repetitions of the free vibration tests are conducted to assure precision, using a modal analysis tool to compute the Frequency Response Function (FRF), damping ratio, and fundamental frequencies of the material. This thorough method not only improves the comprehension of the aluminum-alumina composite but also offers insights into its long-term performance and stability under operating settings.

2.3 Special Relativity Search Optimized Long Short-Term Memory Modelling

The Special Relativity Search Modelling Approach is a computational methodology designed to analyze and predict the behavior of systems in high-velocity scenarios, where the principles of special relativity become significant. The process begins with defining the physical system under investigation and identifying the key parameters that influence its behavior, such as rotational speed, number of passes, and transverse speed in friction stir processing.

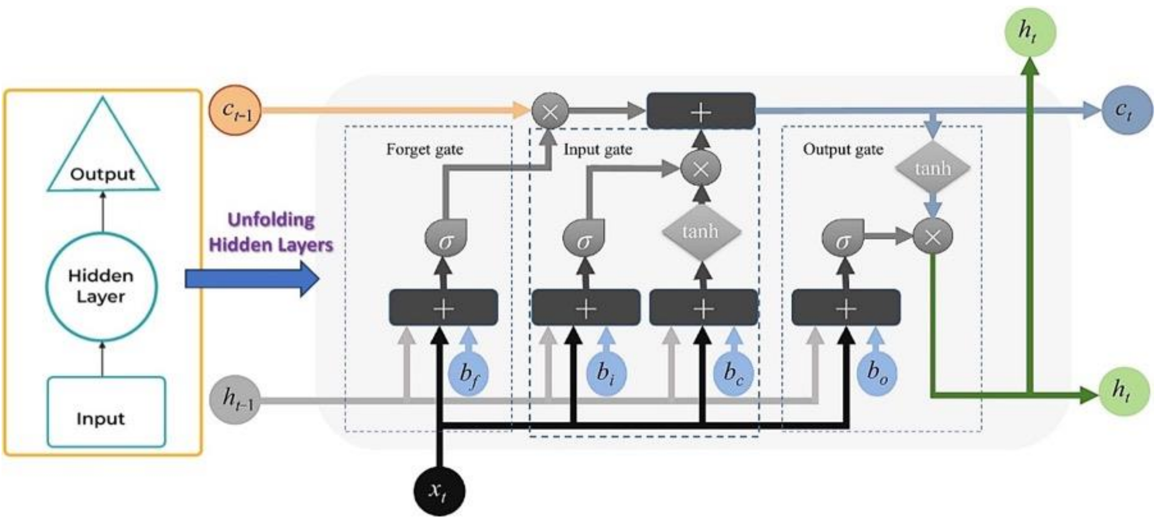

Fig. 4. Systematic View of LSTME Network

SRS modelling approach incorporates several key components that facilitate the analysis and prediction of phenomena in high-velocity scenarios governed by the principles of special relativity. Here are the essential components of the SRS approach:

2.3.1 Relativistic Equations

The foundation of the SRS approach is built upon the equations of special relativity, such as the Lorentz transformations. These equations describe how measurements of time, length, and velocity are affected for observers in different inertial frames, allowing for accurate modeling of relativistic effects.

2.3.2. Parameter Identification:

Clearly defining and identifying the key parameters that influence the behavior of the system under investigation is crucial. This includes variables such as velocity, energy, momentum, and mass, which must be considered to understand how they interact within a relativistic framework.

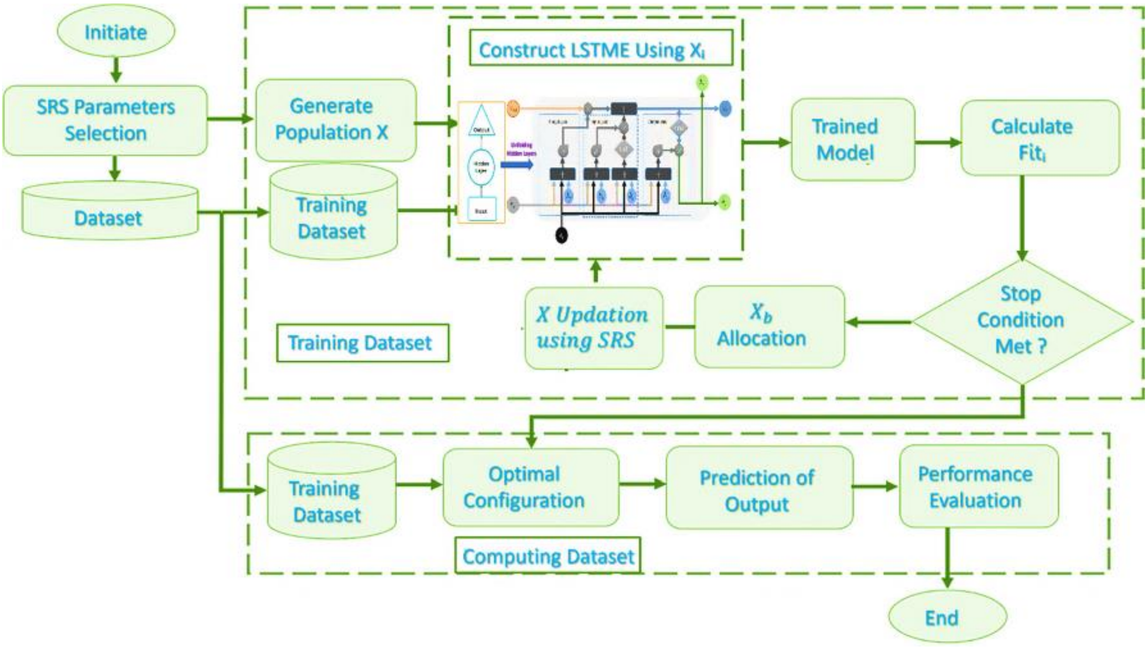

Fig. 5. Special Relativity Search-based LSTME Network Model

2.3.3 Data Collection

Gathering data relevant to the system being modeled is a critical component. This may involve experimental measurements or numerical simulations that reflect the system's behavior at relativistic speeds. The quality and comprehensiveness of this data are vital for model accuracy.

2.3.4 Model Development:

In the SRS approach, a computational model is developed to represent the relationships between input parameters and output behaviors based on the principles of special relativity. This model can utilize techniques from statistics, machine learning, or traditional numerical methods to approximate the system's response.

2.3.5 Optimization Techniques

The SRS approach employs optimization algorithms to explore the parameter space effectively. By systematically varying input parameters, the model identifies optimal conditions that maximize or minimize desired outcomes, such as efficiency or performance in relativistic contexts.

2.3.6 Simulation and Analysis:

Once the model is established, simulations are conducted to predict system behavior under various scenarios. This allows for the examination of how relativistic effects, such as time dilation and length contraction, influence the outputs.

2.3.7 Validation

A critical step in the SRS approach involves validating the model's predictions against independent experimental results or established theoretical benchmarks. This ensures that the model accurately captures the dynamics of the relativistic system.

3. Results and Discussions

The study's findings, depicted in Figures 6-8, clearly establish a direct correlation between the FSP Parameters and damping ratio. Nevertheless, the capacity to diminish vibrations can be improved at a particular optimal rotational velocity.

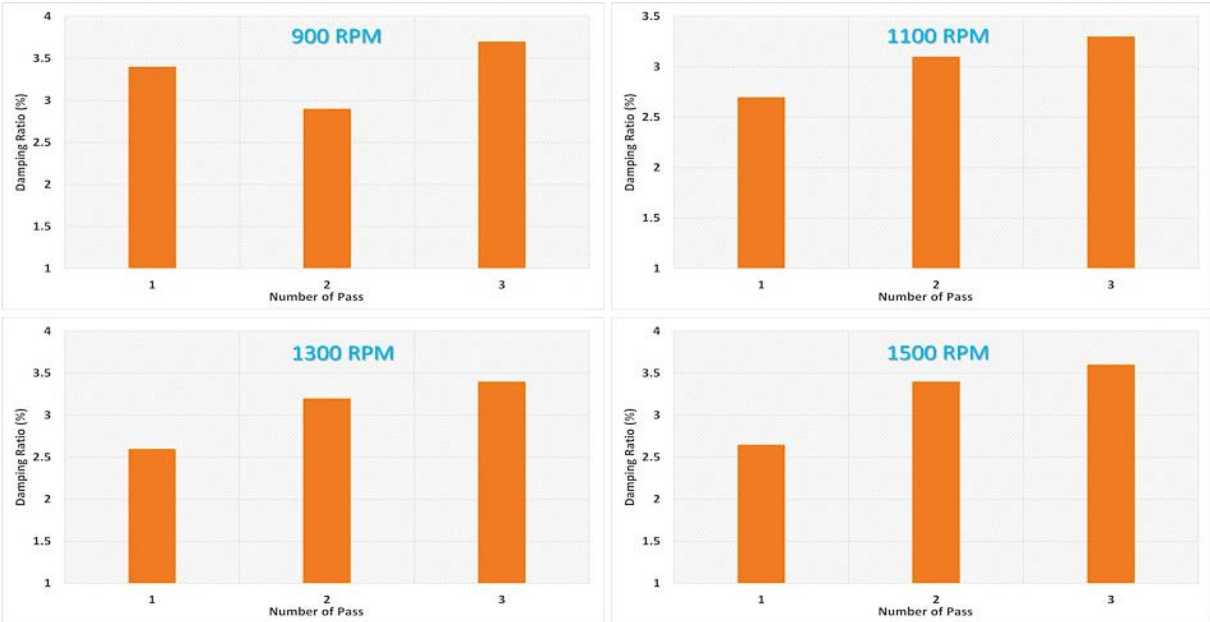

Fig. 6. Damping capacity of the samples at a traverse speed of 10 mm/min.

The data illustrates the influence of rotational speed (RPM) and the number of passes on the damping ratio of an aluminum alloy processed through friction stir processing (FSP) at a consistent traverse speed of 10 mm/min. At 1000 RPM, the damping ratio increases as the number of passes rises, reaching 3.68% after three passes. Similarly, at 1200 RPM, the damping ratio improves with additional passes, peaking at 3.43% with three passes. However, an interesting trend emerges at 1400 RPM, where the highest damping ratio of 4.62% occurs at two passes, suggesting an optimal setting for vibration reduction at this speed. In contrast, at 1600 RPM, the damping ratio fluctuates less significantly, increasing modestly with more passes but not reaching the levels observed at 1400 RPM. Overall, the findings indicate that both RPM and the number of passes play critical roles in determining the damping ratio, with an optimal combination observed at 1400 RPM and two passes [33]–[35].

The data at a traverse speed of 15 mm/min shows the impact of varying rotational speeds (RPM) and the number of passes on the damping ratio. At 1000 RPM, the damping ratio increases significantly with the second pass, reaching a peak of 4.74%, before slightly decreasing to 3.86% with the third pass. This indicates an optimal damping performance at two passes. At 1200 RPM, the damping ratio gradually improves with additional passes, increasing from 2.72% after the first pass to 3.27% after the third pass. For 1400 RPM, the damping ratio initially dips to 3.34% at two passes but rises to 4.43% at three passes, suggesting enhanced vibration reduction with increased processing passes at this speed. However, at 1600 RPM, the damping ratio does not follow a consistent trend; it begins at 3.09% for the first pass, drops to 2.41% at two passes, and rises to 3.37% at three passes.

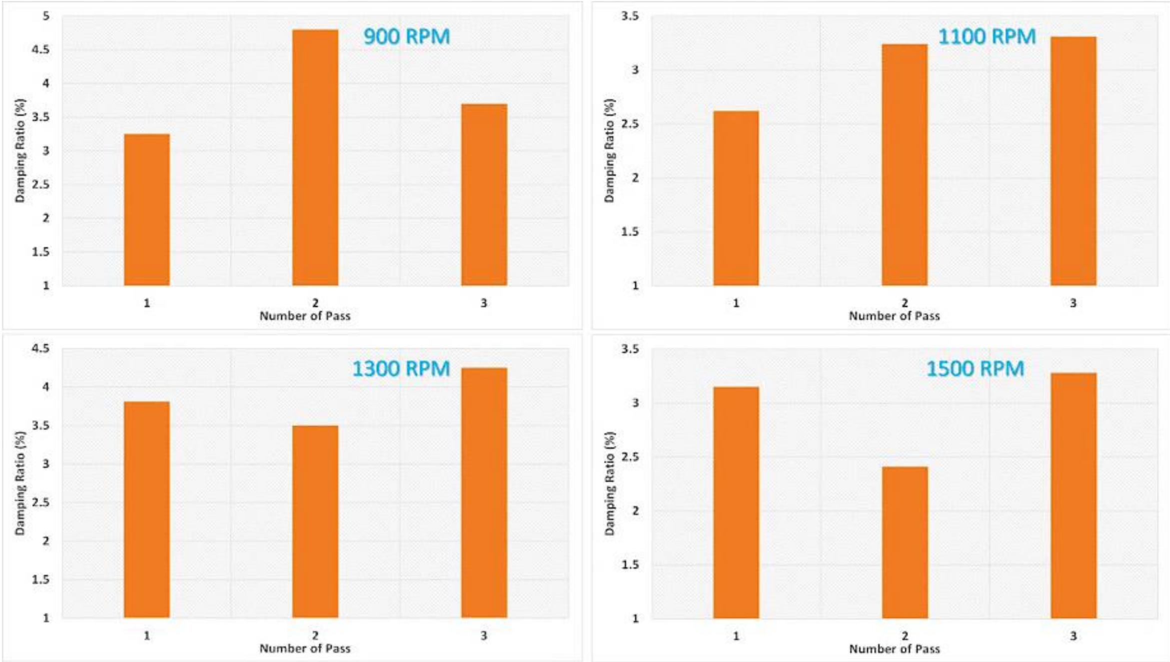

Fig. 7. Sample's damping ratio at 15 mm/min traverse speed

The data at a traverse speed of 20 mm/min reveals how rotational speed (RPM) and the number of passes affect the damping ratio. At 1000 RPM, the damping ratio increases significantly with two passes, reaching 4.48%, before slightly decreasing to 3.02% with the third pass. This suggests an optimal damping effect with two passes at this speed. For 1200 RPM, the damping ratio is initially high at 3.47% for the first pass and reaches a maximum of 3.59% at two passes before dropping to 2.97% at the third pass. At 1400 RPM, there is a notable decrease from 3.11% after the first pass to 2.39% at two passes, with a slight recovery to 2.76% after the third pass.

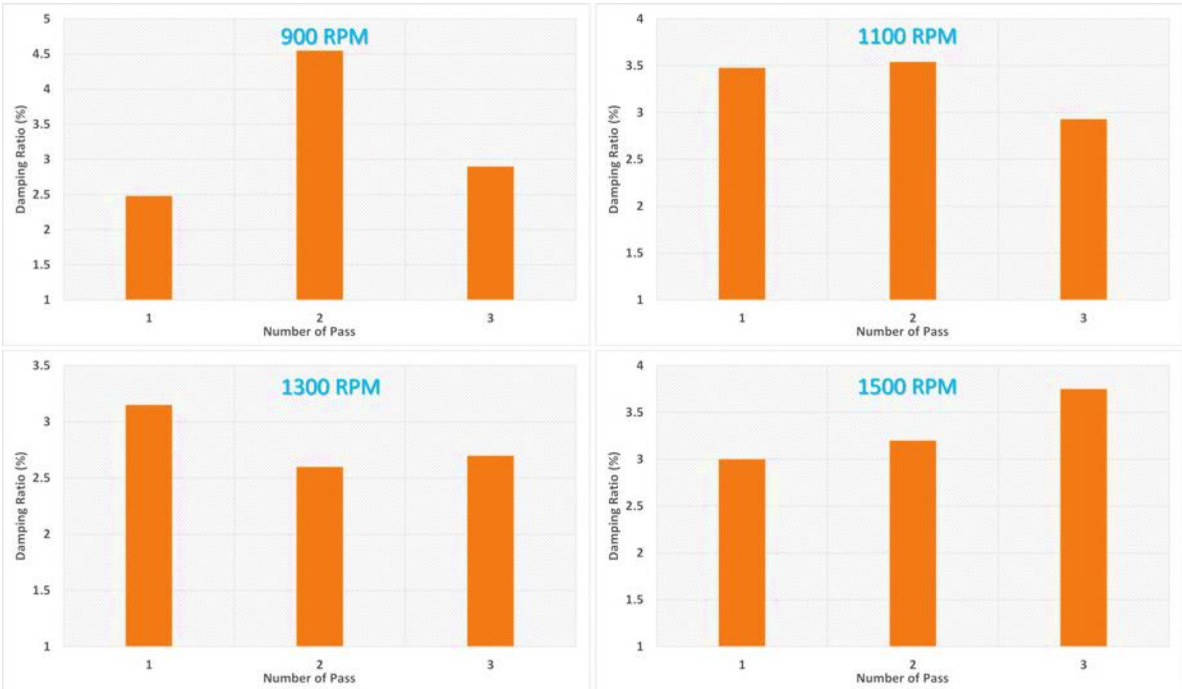

Fig. 8. Damping capacity of the samples at a traverse speed of 20 mm/min.

Meanwhile, at 1600 RPM, the damping ratio gradually increases from 3.05% at one pass to 3.74% at three passes, indicating improved damping properties with more passes at higher speeds. Overall, these results show that both RPM and the number of passes influence the damping performance, with the best performance observed at 1000 RPM with two passes and at 1600 RPM with three passes under a traverse speed of 20 mm/min.

The samples' natural frequency drops according to the increase in the number of passes. The instrument's recurring agitation causes the disintegration of material particles, leading to a loss in stiffness and the subsequent generation of this phenomenon. On the other hand, increasing the number of passes leads to samples that have a greater damping ratio. The agitating movement enhances the grain structure, hence augmenting the presence of imperfections and enhancing its efficacy in catching and absorbing vibrations. Similarly, when the number of passes grows, the sample loss factor also increases. The reason for the increase in frictional losses is due to the presence of a more precise grain structure. The loss factor, on the other hand, quantifies the amount of energy that is converted into heat during vibration. Also, the retained modulus of samples drops with increasing pass count. Deterioration of the grain structure, which results in reduced elasticity, is a likely cause. If we increase the number of passes, we get a similar trend in the samples' loss modulus. The fundamental rationale for this occurrence is provided by the loss modulus, which measures the energy dissipation that occurs during vibration; materials with finer grain patterns show bigger levels of frictional losses.

Table 2. Significant process parameters of the FSP Process [36-38]

Rotational Speed	Number of Passes	Transverse Speed	Damping Ratio (ζ)	Loss Factor	Shear Modulus
1100 rpm	3	20 mm/min	2.98	0.058	26.12 MPa
900 rpm	3	15 mm/min	3.57	0.072	25.91 MPa

Table 2 provides a concise overview of the variations in the dynamic characteristics of the samples at various RPMs. Rotational speed plays a crucial role in determining the heat generation and plastic deformation during the Friction Stir Processing (FSP) process. At a higher rotational speed of 1100 rpm, the damping ratio is lower (2.98%) compared to 3.57% at 900 rpm. This reduction in damping ratio at higher speeds can be attributed to the increased thermal input, which may result in finer grain structures but potentially reduces the material's ability to dissipate energy. The loss factor, which represents the material's capacity to absorb vibrational energy, is also lower at 1100 rpm (0.058) than at 900 rpm (0.072), indicating that slower rotational speeds may enhance energy dissipation. In both cases, three passes were used. Multiple passes generally improve the homogeneity of the processed zone and help in refining the microstructure further. A refined and homogeneous microstructure often leads to improved mechanical properties, such as better damping characteristics and enhanced shear modulus. Thus, conducting multiple passes ensures a more uniform material structure, leading to consistent mechanical property results across different speeds. The transverse or traverse speed, which represents the tool's movement along the workpiece, influences the heat input and material flow characteristics. A slower traverse speed (15 mm/min) allows for more heat accumulation, potentially resulting in a softer, more ductile material, as seen with the higher damping ratio (3.57%) and loss factor (0.072) at this speed. In contrast, a faster traverse speed (20 mm/min) reduces the heat input per unit length, leading to a relatively lower damping ratio (2.98%) and loss factor (0.058). This difference is because the lower heat input at higher traverse speeds tends to produce a stiffer material structure, slightly decreasing its ability to dissipate vibrational energy. The shear modulus values are relatively close for both conditions (26.12 MPa at 1100 rpm and 25.91 MPa at 900 rpm), though a slight increase is observed at the higher speed of 1100 rpm. This suggests that the stiffer material structure obtained at higher rotational and transverse speeds may slightly enhance the shear modulus. However, the difference is not substantial, indicating that the FSP process has a limited but positive impact on shear modulus at these parameter settings.

3.1 Mechanical Properties

In friction stir surface processing (FSP), the primary mechanism that strengthens the material is grain refinement. By using a rotating tool to generate heat and mechanical deformation, FSP produces a fine, uniform grain structure, which directly impacts the mechanical properties of the material. Initially, the Al-6061 alloy has a relatively coarse grain structure, with an average grain size of about 142 μm and an aspect ratio of 32.3%. Grain size and aspect ratio are key factors in determining the mechanical behavior of metals: smaller, more equiaxed (rounded) grains generally improve strength and ductility. After three passes of FSP, the grain size is reduced to just 12.92 μm, and the aspect ratio increases to 91.8%, indicating that the grains are now more uniform and compact. This fine-grained structure enhances the material's mechanical performance by creating more grain boundaries, which act as barriers to dislocation movement (dislocations are defects in the crystal structure that lead to deformation).

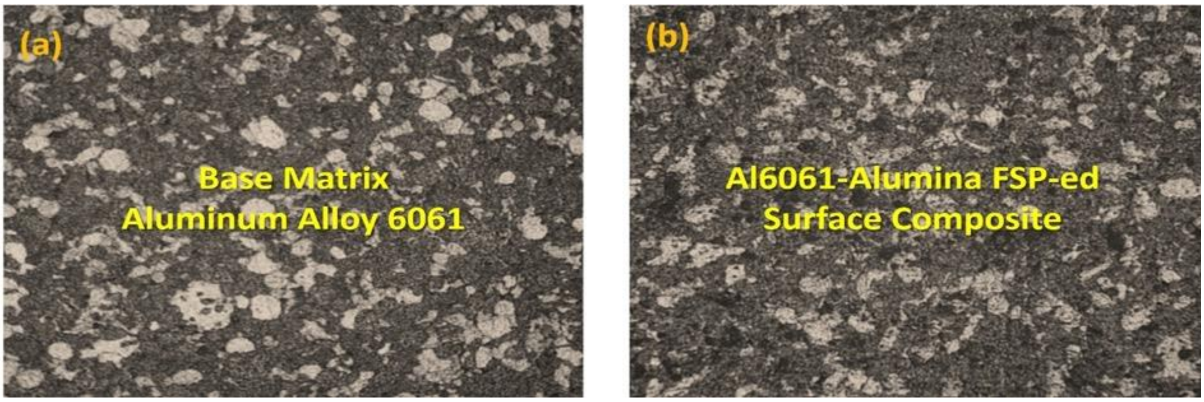

Fig. 9. Optical microscope analysis (a) Base Alloy and (b) FSP-ed Composite

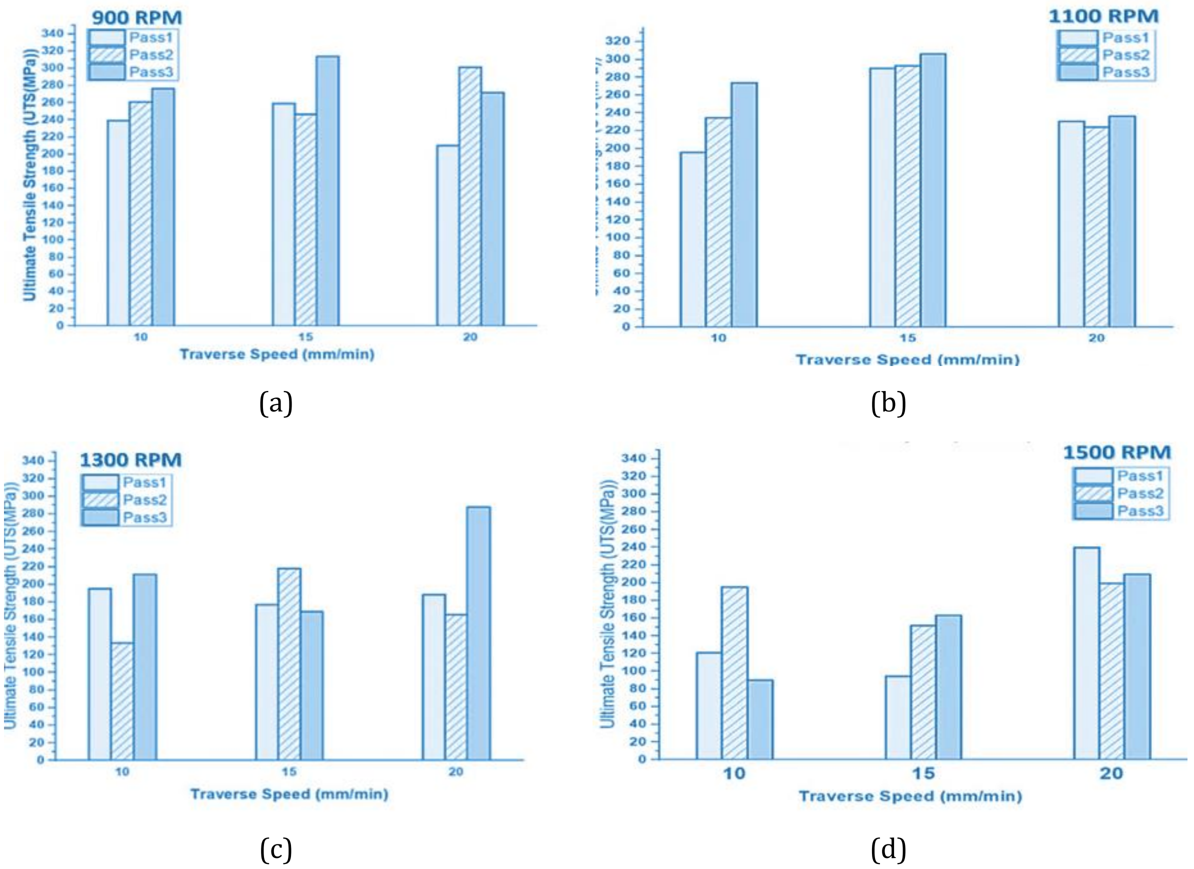

Fig. 10. Tensile Strength of the specimens at different RPM (a) 900 RPM, (b) 1100 RPM, (c) 1300 RPM and (d) 1500 RPM

The microstructure images in Figure 9 confirm this refinement, showing that FSP successfully produces a finer grain structure. This refined microstructure has a direct impact on the material's ultimate tensile strength (UTS) and yield strength (YS). The findings suggest that as the rotational speed of the FSP tool increases, more heat is generated, which facilitates dynamic recrystallization—a process where the grains are continuously broken down and reformed into smaller grains. The combination of heat and mechanical action at higher speeds accelerates this process, leading to a more uniform microstructure and, consequently, stronger material properties. Higher rotational speeds not only refine the grain structure but also improve the material's resistance to deformation, enhancing its yield strength. A finer microstructure limits dislocation motion and requires greater force to initiate plastic deformation, thereby increasing yield strength. This makes the material stronger and more durable, as it can withstand greater forces before it starts to deform. In summary, the increased rotational speeds in FSP contribute to a more refined grain structure, which strengthens the material by impeding dislocation movement, enhancing both UTS and YS.

The observed decrease in yield strength (YS) and ultimate tensile strength (UTS) with an increasing number of FSP passes can be understood in terms of the effects of excessive grain refinement and heat input. In FSP, each pass of the tool applies heat and mechanical agitation to the material, breaking down grains and refining the microstructure. However, after a certain point, too many passes can lead to over-processing of the material. With repeated agitation, the grains can become excessively fragmented, which may lead to the formation of ultra-fine or even amorphous regions that lack the cohesive crystal structure needed to maintain high strength. In a finely grained microstructure, dislocations (defects within the crystal lattice) have a harder time moving, which generally improves strength. However, if the grains become too small or disordered, the material may lose its ability to effectively carry loads due to compromised grain boundaries, which weakens its structural integrity and leads to a reduction in YS and UTS. Similarly, reducing the feed rate (i.e., slowing down the tool's movement across the surface) increases the duration of heat exposure per unit area. This slower rate of travel means that heat dissipates more slowly, allowing for prolonged thermal exposure. When the material remains hot for too long, it can cause excessive grain growth or even coarsening in some cases, leading to a reduction in strength. Prolonged heating also reduces the effectiveness of grain boundary strengthening, as it allows grains to relax or reorient in ways that make them less resistant to deformation [39]–[41].

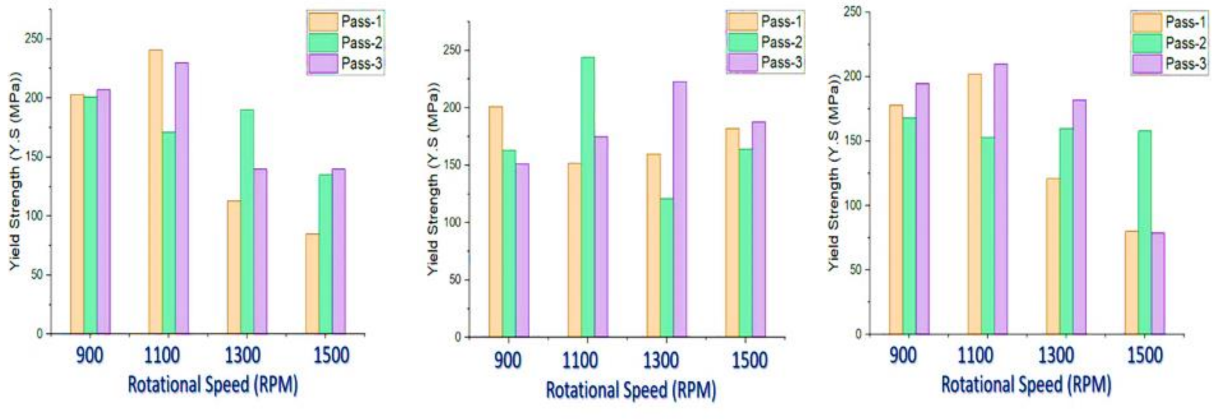

Fig. 11. Yield Strength of the specimens at different RPM and no. of pass

3.2 Predicted Results

The research effort focuses on employing four distinct machine-learning models to predict specific features of processed data, including Ultimate Tensile Strength (UTS), Yield Strength (YS), natural frequency, and damping ratio.

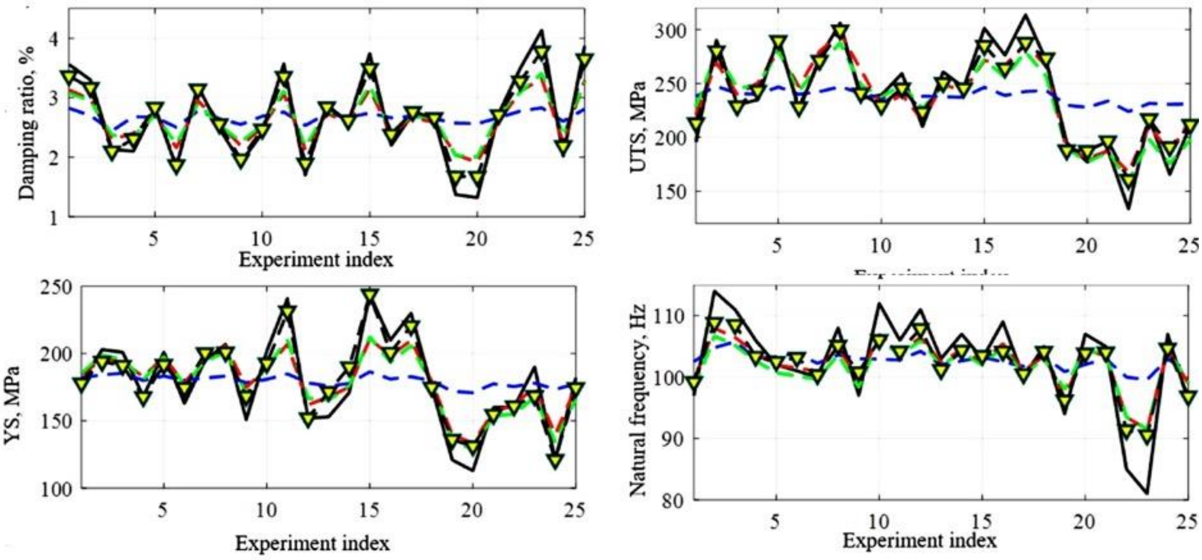

Fig. 12. Training process of experimental and predicted data

The first model is an independent Long Short-Term Memory (LSTM) model, which learns to make predictions based solely on the input data without any additional optimization techniques. The following three models build upon the LSTM framework by incorporating various optimization approaches. These optimized models include LSTME-FHO, which enhances the LSTM with the Firefly Algorithm, LSTME-SRS that utilizes Particle Swarm Optimization, and LSTME-DMOA, which applies the Differential Multi-Objective Algorithm for optimization.

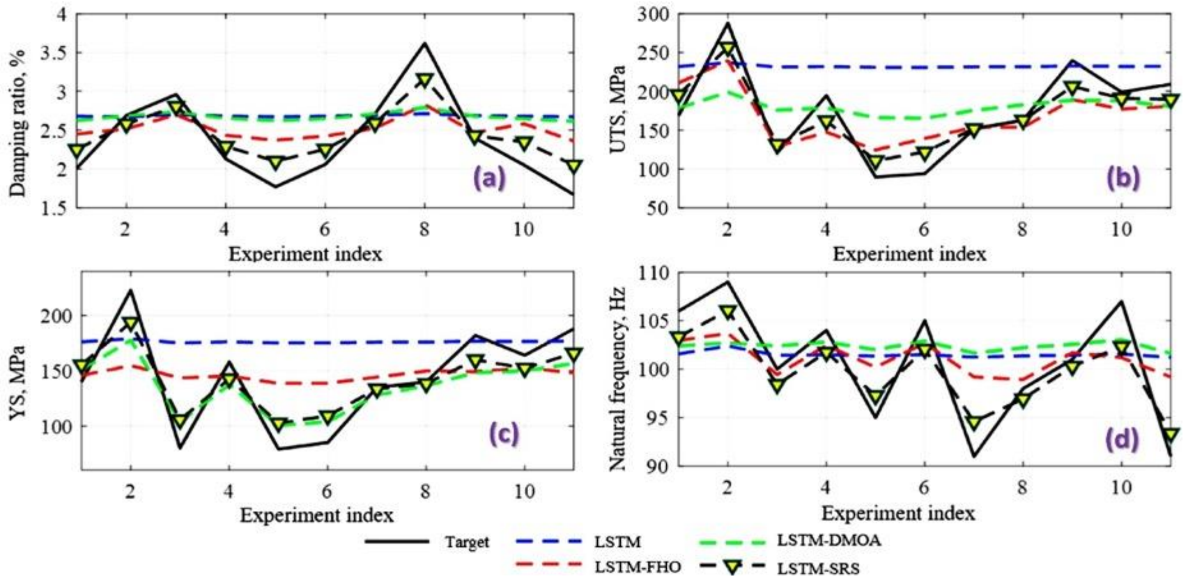

Fig. 13. Testing process of experimental and predicted data

To evaluate the models' performance, empirical data is divided into two parts: 70% of the data is allocated for training the models, allowing them to learn patterns and adjust their parameters, while the remaining 30% is reserved for testing, which assesses how well the trained models can predict outcomes for unseen data. The effectiveness of each model is measured using three accuracy metrics: Root Mean Square Error (RMSE), which quantifies the difference between predicted and actual values; Coefficient of Determination (R^2), reflecting the proportion of variance in the dependent variable explained by the independent variables; and Mean Absolute Error (MAE), which indicates the average absolute differences between predictions and actual values. Through this research, the aim is to enhance prediction accuracy for important engineering characteristics by exploring the capabilities of various machine-learning models and their optimization technique.

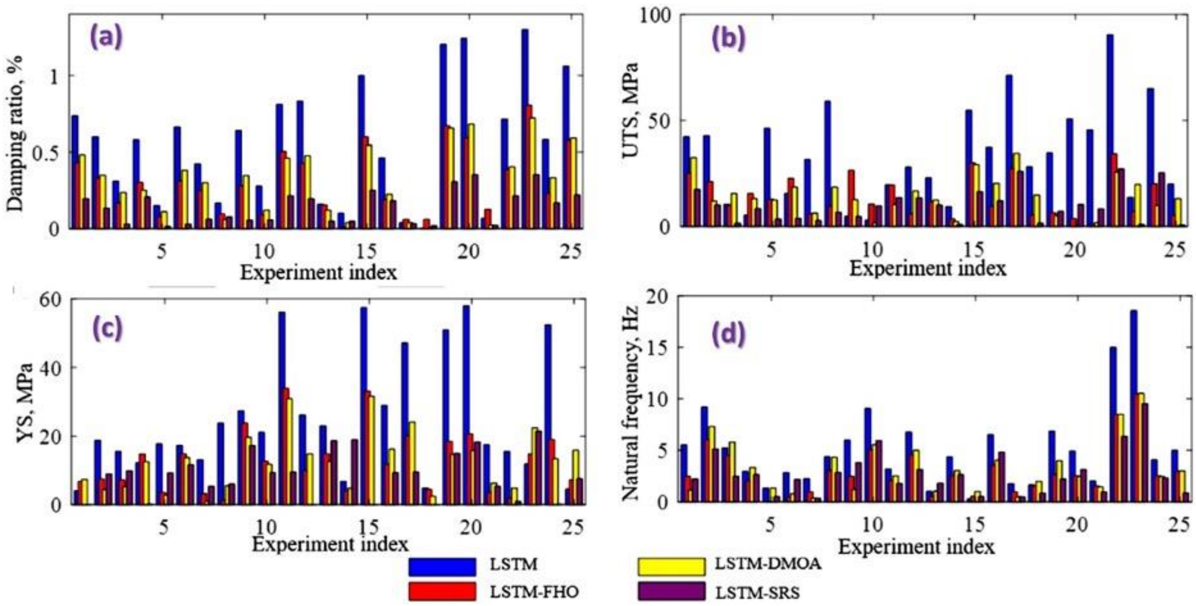

Fig. 14. Training processing error of experimental and predicted data

The findings of the research demonstrate a strong correlation between the experimentally acquired data and the predicted outcomes generated by the machine learning models. Among the models tested, the LSTME-SRS model outperformed all others, indicating its effectiveness in making accurate predictions. It was followed closely by the LSTME-DMOA and LSTME-FHO models, which also showed commendable performance. In contrast, the independent LSTM model consistently exhibited the least alignment with the experimental data during both the training and testing phases, indicating its limitations in capturing the underlying patterns in the data. Furthermore, an analysis of absolute errors revealed that the LSTME-SRS model maintained the lowest error across all characteristics examined, reinforcing its superior predictive power. This consistent performance supports the earlier findings of strong correlation. Additionally, when comparing the absolute errors of the LSTME-SRS model with those of the LSTM model, it was noted that the errors produced by the LSTME-DMOA and LSTME-FHO models were relatively small, although they did not surpass the accuracy of the LSTME-SRS.

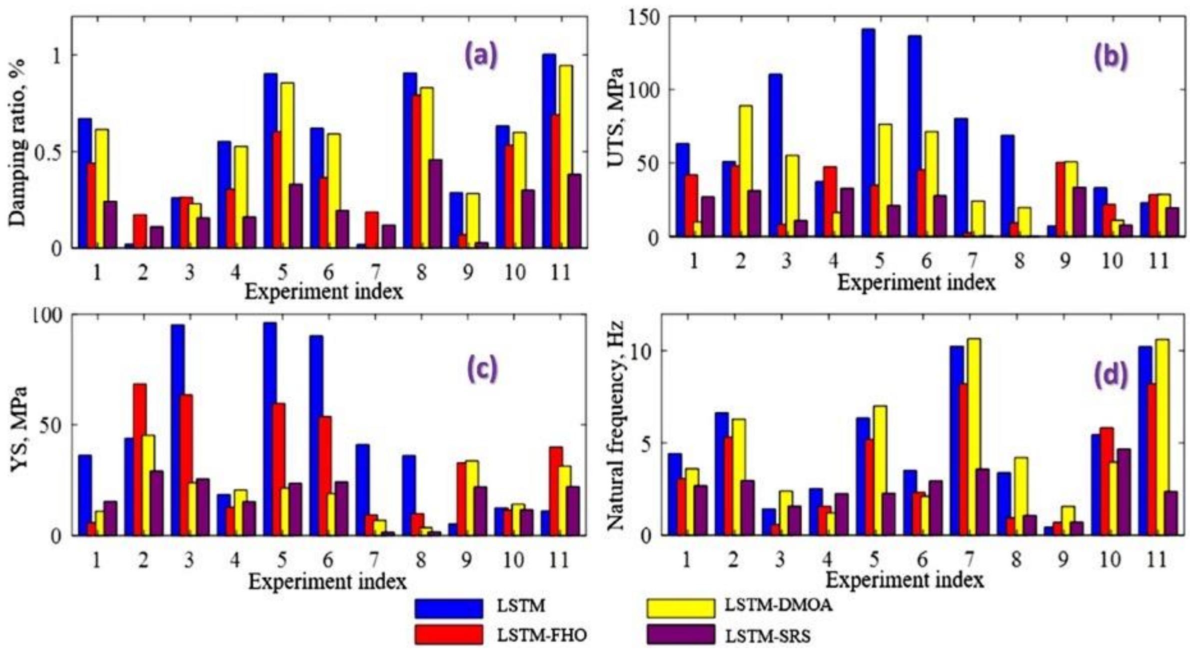

Fig. 15. Testing processing error of experimental and predicted data

Overall, these results highlight the efficacy of optimization techniques in enhancing the predictive capabilities of LSTM models, particularly the advantages offered by the LSTME-SRS approach. The LSTME-SRS algorithm exhibits exceptional efficacy in accurately predicting various attributes of processed data, as evidenced by its ability to generate minimal absolute error in predictions. The results of this study indicate that LSTME-SRS consistently outperforms the other models in terms of predictive accuracy, highlighting its capability to effectively anticipate the features of the processed data.

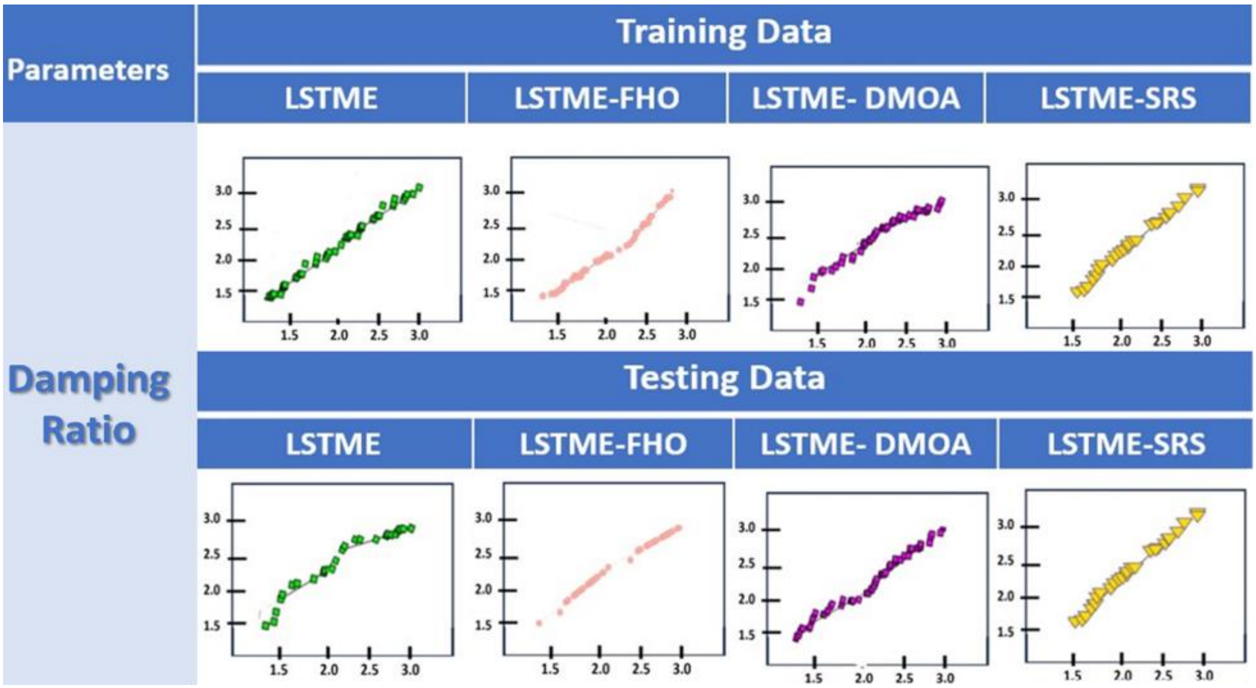

Fig. 16. QQ plots for damping ratio during training and testing of data

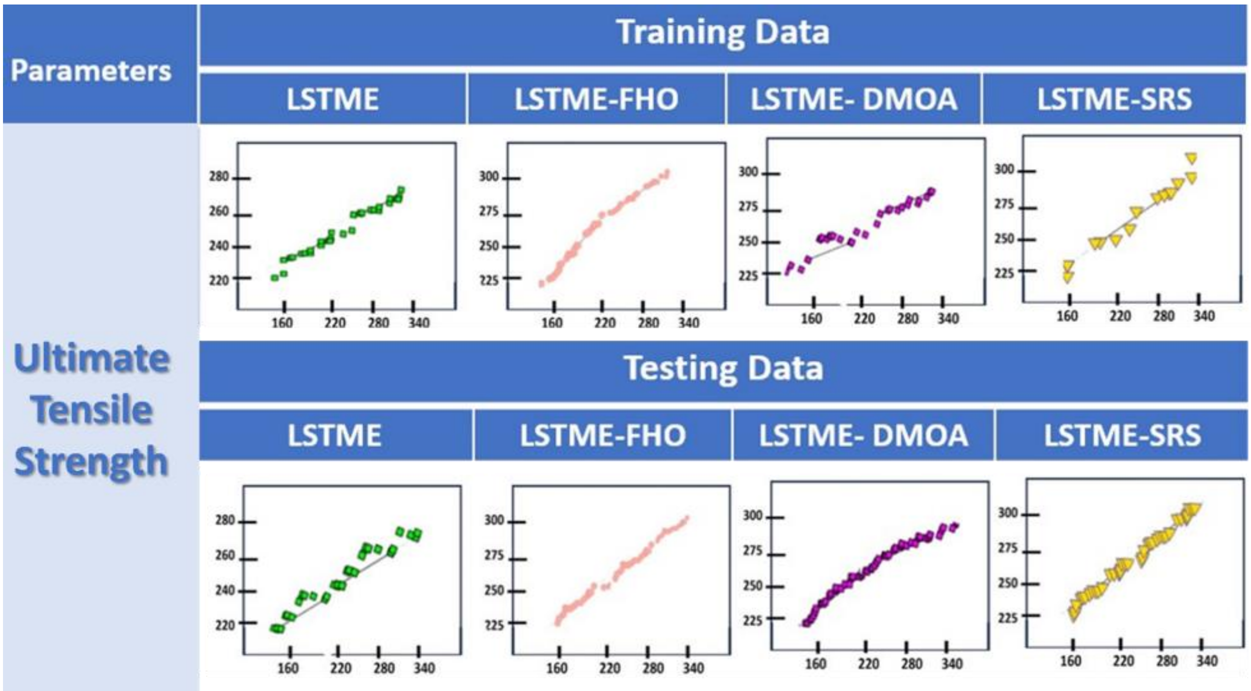

Fig.17. QQ plots for ultimate tensile strength during training and testing of data

When comparing the QQ (Quantile-Quantile) plots illustrated in Figures 16-19, it becomes apparent that there is a stronger correlation between the predicted and actual data for the LSTME-DMOA and LSTME-FHO models when assessed against the LSTME-SRS model. This suggests that while LSTME-SRS remains the top performer, the LSTME-DMOA and LSTME-FHO models also establish a relatively robust relationship with the experimental data. The QQ plots provide a visual representation of how closely the predicted values align with the actual values, reinforcing the findings that LSTME-SRS is superior in accuracy, but indicating that the other two models still maintain meaningful predictive capabilities.

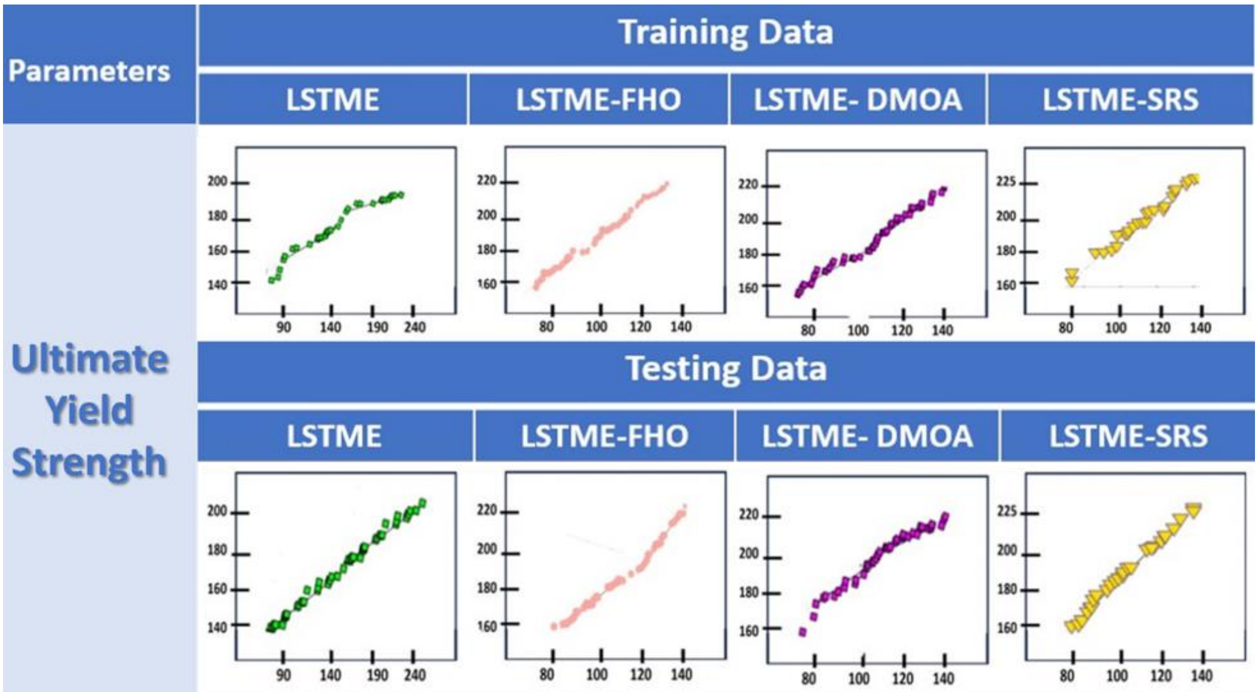

Fig. 18: QQ plots for ultimate yield strength during training and testing of data

Fig. 19. QQ plots for natural frequency during training and testing of data

The predictive accuracy of the LSTME-SRS model is evidenced by the close proximity of its predicted outcomes—represented in yellow—to the diagonal lines on the plot, which typically signify ideal predictions where the predicted values match the actual experimental results perfectly. In contrast, the predictions generated by the independent LSTM model, depicted in a light green, show a greater deviation from these diagonal lines, highlighting its poorer performance and accuracy. This noticeable disparity in prediction accuracy further reinforces the conclusion that the LSTME-SRS model significantly outperforms the independent LSTM, LSTME-FHO, and LSTME-DMOA models. The assessment of model performance through various metrics—such as the coefficient of determination (R^2), mean absolute error (MAE), and root mean square error (RMSE)—further substantiates the findings. These metrics quantitatively confirm that LSTME-SRS consistently yields higher accuracy, characterized by lower error values and a stronger fit to the experimental data, distinguishing it as the most reliable model among those tested[1], [42], [43].

Table 3 presents the results in a concise format for your convenience. The provided data highlights the performance metrics of four machine learning models—LSTME-SRS, LSTME-FHO, LSTME-DMOA, and the independent LSTM model—across four different predictive tasks: damping ratio (ζ), natural frequency, ultimate tensile strength (UTS), and yield strength (YS). The metrics evaluated include the coefficient of determination (R^2), root mean square error (RMSE), and mean absolute error (MAE) for both training and testing datasets. For the damping ratio, the LSTME-SRS model achieved an impressive R^2 value of 0.992 during training, indicating a strong fit to the data, and maintained a high R^2 of 0.985 during testing. Its RMSE and MAE values were also the lowest among all models, demonstrating superior predictive accuracy. The LSTME-DMOA model followed closely with an R^2 of 0.999 in training, although its RMSE and MAE were slightly higher, indicating some discrepancy in predictions. The LSTME-FHO model, while still effective, showed lower performance, particularly in testing with an R^2 of 0.823, highlighting its limitations in capturing the damping ratio accurately. In stark contrast, the independent LSTM model exhibited the weakest performance, with the lowest R^2 values and highest error metrics across both training and testing phases.

Table 3. Machine-learning model and performance measures

Properties	Models	Training Data			Testing Data		
		R^2	RMSE	MAE	R^2	RMSE	MAE
Damping ratio (ζ)	LSTME-SRS	0.992	0.172	0.138	0.985	0.258	0.227
	LSTME-FHO	0.988	0.374	0.307	0.823	0.459	0.405
	LSTME-DMOA	0.999	0.387	0.316	0.977	0.589	0.499
	LSTME	0.746	0.688	0.564	0.724	0.629	0.5336
Natural Frequency (Hz)	LSTME-SRS	0.977	2.803	2.221	0.952	2.684	2.463
	LSTME-FHO	0.964	5.756	4.456	0.710	4.692	3.805
	LSTME-DMOA	0.923	5.582	4.413	0.845	5.846	4.876
	LSTME	0.668	6.674	5.234	0.541	5.837	4.959
Ultimate Tensile Strength (MPa)	LSTME-SRS	0.964	12.384	9.687	0.911	22.706	19.277
	LSTME-FHO	0.899	16.783	1.392	0.704	65.103	30.723
	LSTME-DMOA	0.895	17.003	14.367	0.885	49.306	41.109
	LSTME	0.788	40.766	34.120	0.721	80.692	68.359
Yield Strength (MPa)	LSTME-SRS	0.966	10.824	8.497	0.953	19.583	17.439
	LSTME-FHO	0.902	15.367	12.518	0.756	40.784	33.336
	LSTME-DMOA	0.943	15.062	12.573	0.934	24.016	20.947
	LSTME	0.882	30.660	25.271	0.861	55.020	44.185

In predicting natural frequency, the LSTME-SRS model again led the pack with an R^2 of 0.977 during training and 0.952 in testing, along with relatively low RMSE and MAE values. The LSTME-FHO and LSTME-DMOA models performed adequately but had noticeably higher errors, indicating a greater challenge in accurately predicting this characteristic compared to the damping ratio. The independent LSTM model struggled here as well, with a low R^2 of 0.541 in testing. When assessing ultimate tensile strength, the LSTME-SRS model continued to perform strongly with an R^2 of 0.964 in training, although the RMSE and MAE were considerably higher than in previous metrics, suggesting the inherent complexity of this prediction task. The LSTME-FHO and LSTME-DMOA models showed significant errors during testing, especially the LSTME-FHO, which had an RMSE of

65.103, indicating a poor fit for UTS predictions. Again, the independent LSTM model showed the least effectiveness, reflected in its high error metrics. Lastly, for yield strength, the LSTME-SRS model again outperformed the others with an R^2 of 0.966 in training and 0.953 in testing, coupled with lower RMSE and MAE values, affirming its reliability. The LSTME-DMOA model also performed well, though it showed a slight increase in error metrics compared to its training performance. The independent LSTM model's performance remained consistently poor across all tasks. Overall, the results clearly indicate that the LSTME-SRS model is the most effective among the models tested, achieving high R^2 values and low error metrics across various characteristics. The integration of optimization techniques in models like LSTME-FHO and LSTME-DMOA enhances predictive accuracy compared to the independent LSTM model, yet they still fall short of the performance demonstrated by LSTME-SRS, particularly in more complex prediction tasks like ultimate tensile strength and yield strength.

4. Conclusions

The study introduces a novel approach to predicting the mechanical properties of aluminum alloys processed through friction stir processing (FSP) by employing a Special Relativity Search Optimized Long Short-Term Memory (LSTME-SRS) model. This study employed a CNC milling machine to conduct friction stir processing on Al-6061 aluminum alloy, utilizing aluminum oxide nanoparticles as reinforcements. The incorporation of alumina nanoparticles and controlled adjustments to FSP parameters, such as rotational speed and the number of passes, significantly impacted the material's damping capacity, yield strength, and tensile strength. Using a machine learning approach, specifically the SRS-optimized LSTME model, provided highly accurate predictions of these properties, which validated the experimental findings and highlighted the effectiveness of the optimization. The following conclusions were mentioned as follows:

- The highest damping capability was achieved with a rotational speed of 900 rpm and a traverse speed of 15 mm/min, where the damping ratio (ζ) reached 3.57, and the loss factor was 0.072.
- This optimal condition allowed the material to absorb and mitigate vibrations more effectively, largely due to a fine and evenly dispersed grain structure, enhanced by alumina nanoparticle reinforcement.
- Higher rotational speeds led to increased thermal energy, which refined the grain structure and made the material stronger yet less rigid.
- The shear modulus decreased to 25.91 MPa at 900 rpm and further dropped at higher rotational speeds, indicating a balance between strength and flexibility as rotational speed increased.
- Increased rotational speeds improved yield strength (YS) and ultimate tensile strength (UTS). The optimized LSTME model achieved R^2 values of 0.953 for YS and 0.911 for UTS, demonstrating a strong correlation between speed and material strength. This improvement results from grain refinement, which increased resistance to deformation.
- The SRS-optimized LSTME model excelled in prediction accuracy, outperforming other models with R^2 values between 0.911 and 0.992 for UTS, YS, natural frequency, and damping ratio.
- The SRS optimization reduced the root mean square error (RMSE) and mean absolute error (MAE) by up to 71.86% and 71.61%, respectively. This demonstrates the model's robustness in forecasting material properties effectively.
- More friction-stir processing passes led to a reduction in natural frequency and stiffness, while increasing the damping ratio and loss modulus. With more passes, energy dissipation during vibrations increased, as reflected by a rise in the loss modulus, which indicates more effective damping capability. Each pass further refined the grain structure, enhancing the presence of microscopic imperfections that improved vibration absorption.
- With increased RPM, there was a noted rise in damping capacity, as the refined grain structure introduced by higher rotational speeds enabled the material to better absorb and dissipate energy. The data suggest that higher thermal energy generation during FSP aids grain breakdown, yielding a finely tuned microstructure ideal for high damping applications.

- The friction-stir processing led to significant grain refinement, reducing the average grain size from an initial 142 µm to 12.92 µm after three FSP passes, and increasing the aspect ratio from 32.3% to 91.8%. This transformation in microstructure substantially improved the material's strength and deformation resistance.

5. Applications

- Al-6061/alumina composites are suitable for airplane frames, fuselage structures, and engine parts due to their lightweight and high strength. The LSTME-SRS model predicts and optimizes mechanical parameters, improving performance and fuel economy.
- Advanced composites increase vehicle performance by decreasing weight and preserving strength and durability. Structural components, chassis sections, and body panels may benefit from improved damping for ride comfort and noise reduction.
- High-performance sporting equipment including bicycle frames, golf clubs, and tennis rackets used advanced composites. Composites' lightweight and enhanced mechanical qualities help shock absorption and vibration damping.
- Construction companies use the study's findings to create lightweight, robust materials for buildings, bridges, and other infrastructure. Processing parameters enhance mechanical properties for safer and more efficient designs.
- Al-6061/alumina composites are suited for maritime applications such as boat hulls and harsh environment components because of their corrosion resistance and mechanical strength. These materials are optimized for marine durability and performance using predictive modeling.
- Aluminum composites' biocompatibility and mechanical qualities are used to make medical devices and implants. Predicting and controlling material qualities may improve surgical equipment and prostheses.
- Manufacturing processes may use the LSTME-SRS model to anticipate and optimize FSP parameters in real time. This boosts manufacturing efficiency, eliminates waste, and increases product quality.

6. Future Perspective

- The LSTME-SRS model can be applied to other metal matrix composites (MMCs) and materials besides Al-6061. This demonstrates the model's versatility across numerous material systems, perhaps leading to practical applications.
- Real-time industrial process input may increase predictive model accuracy and adaptability. This connectivity would allow real-time processing setting changes during FSP, improving material properties and production efficiency.
- Tool geometry, cooling methods, and post-processing treatments may affect composite mechanical properties in future study. Understanding these components may enhance material performance.
- Long-term studies on treated materials' durability and fatigue resistance in various environments would provide light on their practical performance. This may help assess the durability and reliability of composite components.
- Hybrid reinforcing systems that combine alumina with nanoparticles or fibers may improve composite mechanical properties. To increase performance, research may focus on reinforcement interactions.
- Machine learning advances may improve LSTME-SRS predictions. Novel algorithms and hybrid models may enhance material quality and processing predictions.

References

[1] Subramani N, Haridass R, Pramodh S, Anand AP, Manikandan N. Mechanical strength analysis of Al6061 & Al2024 based metal matrix composite prepared through stir casting method. Mater Today Proc. 2021;47:4513-7. https://doi.org/10.1016/j.matpr.2021.05.417

[2] Subburaj A, Marcel A, Antony M, Decruz J. Mechanical characterization and micro-structural analysis on AA2024 hybrid composites reinforced with WC and graphene nanoparticles. Trans Indian Inst Met. 2022;75(7):1721-30. https://doi.org/10.1007/s12666-021-02488-z

[3] Kumar D, Singh S, Angra S. Morphology and corrosion behavior of stir-cast Al6061-CeO2 nanocomposite immersed in NaCl and H2SO4 solutions. Evergreen J Carbon Resour Sci Green Asia Strategy. 2023;10(1):94-104. https://doi.org/10.5109/6781054

[4] Kumar D, Kumar R, Thakur L. A review on environment-friendly and lightweight magnesium-based metal matrix composites and alloys. Mater Today Proc. 2020;xxxx. https://doi.org/10.1016/j.matpr.2020.07.424

[5] Yang X, Zhang Y, Huang J, Liu J, Chen J, Li T. Interfacial microstructure evolution and mechanical properties of carbon fiber reinforced Al-matrix composites fabricated by a pressureless infiltration process. Mater Sci Eng A. 2024;891:145968. https://doi.org/10.1016/j.msea.2023.145968

[6] Raja R, et al. Development of Al-Mg2Si alloy hybrid surface composites by friction stir processing: Mechanical, wear, and microstructure evaluation. Materials. 2023;16:4131. https://doi.org/10.3390/ma16114131

[7] Khan MM, Nisar M. Effect of in situ TiC reinforcement and applied load on the high-stress abrasive wear behaviour of zinc-aluminum alloy. Wear. 2022;488-9:204082. https://doi.org/10.1016/j.wear.2021.204082

[8] Ramezani NM, Davoodi B. Evaluating the influence of various friction stir processing strategies on surface integrity of hybrid nanocomposite Al6061. Sci Rep. 2024;xxxx:1-15.

[9] Aydin F. Effect of solid waste materials on properties of magnesium matrix composites: A systematic review. J Magnes Alloys. 2022;xxxx. https://doi.org/10.1016/j.jma.2022.09.005

[10] Konovalova V. The effect of temperature on the corrosion rate of iron-carbon alloys. Mater Today Proc. 2021;38:1326-9. https://doi.org/10.1016/j.matpr.2020.08.094

[11] Saravanan C, et al. Investigation on the mechanical, tribological, morphological and machinability behavior of stir-casted Al/SiC/Mo reinforced MMCs. Mater Today Proc. 2020;21:1-10.

[12] Devanathan C, Babu AS. Friction stir welding of metal matrix composite using coated tool. Procedia Mater Sci. 2014;6:1470-5. https://doi.org/10.1016/j.mspro.2014.07.126

[13] Sharma AK, Bhandari R, Aherwar A, Rimašauskiene R. Matrix materials used in composites: A comprehensive study. Mater Today Proc. 2020;21:1559-62. https://doi.org/10.1016/j.matpr.2019.11.086

[14] Ahmed MR, Moosa A, Ramazani SA, Kubba FA. Synergetic effects of graphene and nonfunctionalized carbon nanotubes hybrid reinforced epoxy matrix on mechanical, thermal and wettability properties of nanocomposites. Am J Mater Sci. 2017;7(1):1-11.

[15] Venkateswarlu K, Ramakrishna K. Recent advances in phase change materials for thermal energy storage: A review. J Braz Soc Mech Sci Eng. 2022;44(1):1-17. https://doi.org/10.1007/s40430-021-03308-7

[16] Kumar S, Kumar A, Vanitha C. Corrosion behaviour of Al7075/TiC composites processed through friction stir processing. Mater Today Proc. 2019;15:21-9. https://doi.org/10.1016/j.matpr.2019.05.019

[17] Reddy PS, Kesavan R, Ramnath BV. Investigation of mechanical properties of aluminium 6061-silicon carbide, boron carbide metal matrix composite. Silicon. 2018;10(2):495-502. https://doi.org/10.1007/s12633-016-9479-8

[18] Kumar D, Singh S, Angra S. Synergistic effects of graphene and ceria nanoparticulates on microstructure and mechanical behavior of stir-cast hybrid aluminum composite. Trans Indian Inst Met. 2024;xxxx:1-15. https://doi.org/10.1007/s12666-024-03368-y

[19] Zheng T, Wang L, Liu J. Corrosion inhibition of levofloxacin and Ce(NO3)3 for AA2024-T4 in 3.5% NaCl. Mater Today Proc. 2020;2782(3):xxxx. https://doi.org/10.1080/1478422X.2019.1681152

[20] Rana H, Badheka V. Influence of friction stir processing conditions on the manufacturing of Al-Mg-Zn-Cu alloy/boron carbide surface composite. J Mater Process Technol. 2018;255:795-807. https://doi.org/10.1016/j.jmatprotec.2018.01.020

[21] Rajkumar V, Venkateshkannan M, Sadeesh P, Arivazhagan N. Studies on effect of tool design and welding parameters on the friction stir welding of dissimilar aluminium alloys AA 5052 - AA 6061. Procedia Eng. 2014;75:93-7. https://doi.org/10.1016/j.proeng.2013.11.019

[22] Ador SH, Kabir S, Ahmed F, Ahmad F, Adil S. Effects of minimum quantity lubrication (MQL) on surface roughness in milling Al Alloy 383/ADC 12 using nano hybrid cutting fluid. 2022;9(4):xxxx. https://doi.org/10.5109/6625790

[23] Sadiq TO, et al. Effect of different machining parameters on surface roughness of aluminium alloys based on Si and Mg content. J Braz Soc Mech Sci Eng. 2019;41(10):1-11. https://doi.org/10.1007/s40430-019-1948-8
[24] Bhatt RJ, Raval HK. Investigation on flow forming process using Taguchi-based grey relational analysis (GRA) through experiments and finite element analysis (FEA). J Braz Soc Mech Sci Eng. 2018;40(11):1-24. https://doi.org/10.1007/s40430-018-1456-2
[25] Hasan MS, Kordijazi A, Rohatgi PK, Nosonovsky M. Application of triboinformatics approach in tribological studies of aluminum alloys and aluminum-graphite metal matrix composites. Miner Met Mater Ser. 2022;1:41-51. https://doi.org/10.1007/978-3-030-92567-3_3
[26] Hasan MS, Wong T, Rohatgi PK, Nosonovsky M. Analysis of the friction and wear of graphene reinforced aluminum metal matrix composites using machine learning models. Tribol Int. 2022;170:107527. https://doi.org/10.1016/j.triboint.2022.107527
[27] Mahajan L, Bhagat S. Machine learning approaches for predicting compressive strength of concrete with fly ash admixture. Res Eng Struct Mater. 2022;xx:1-27.
[28] Prasad KA, John MRS. Optimization of external roller burnishing process on magnesium silicon carbide metal matrix composite using response surface methodology. J Braz Soc Mech Sci Eng. 2021;43(7):1-12. https://doi.org/10.1007/s40430-021-03069-3
[29] Bourkhani RD, Eivani AR, Nateghi HR. Through-thickness inhomogeneity in microstructure and tensile properties and tribological performance of friction stir processed AA1050-Al2O3 nanocomposite. Compos Part B. 2019;174:107061. https://doi.org/10.1016/j.compositesb.2019.107061
[30] Lorenzo-Martin MC, Ajayi OO. Surface layer modification of 6061 Al alloy by friction stir processing and second phase hard particles for improved friction and wear performance. J Tribol. 2014;136(4):1-6. https://doi.org/10.1115/1.4027860
[31] Vedabouriswaran G, Aravindan S. Development and characterization studies on magnesium alloy (RZ 5) surface metal matrix composites through friction stir processing. J Magnes Alloys. 2018;6(2):145-63. https://doi.org/10.1016/j.jma.2018.03.001
[32] Pelevin IA, et al. Selective laser melting of Al-based matrix composites with Al2O3 reinforcement: Features and advantages. 2021;1-18. https://doi.org/10.3390/ma14102648
[33] Aqida SN, Ghazali MI, Hashim J. Effect of porosity on mechanical properties of metal matrix composite: An overview. J Teknol. 2012;40:17-32. https://doi.org/10.11113/jt.v40.395
[34] Casati R, Vedani M. Metal matrix composites reinforced by nanoparticles: A review. 2014;65-83. https://doi.org/10.3390/met4010065
[35] Rajak DK, Pagar DD, Menezes PL, Linul E. Fiber-reinforced polymer composites: Manufacturing, properties, and applications. Polymers. 2019;11(10):xxxx. https://doi.org/10.3390/polym11101667
[36] Kaya N, Çetinkaya C, Karakoç H, Ada H. Effect of process parameters of Al5083/SiC surface composites fabricated by FSP on microstructure, mechanical properties and wear behaviors. Mater Chem Phys. 2024;315:128991. https://doi.org/10.1016/j.matchemphys.2024.128991
[37] Maqbool A, Lone NF, Ahmad T, Khan NZ, Siddiquee AN. Effect of hybrid reinforcement and number of passes on microstructure, mechanical and corrosion behavior of WE43 Mg alloy based metal matrix composite. J Manuf Process. 2023;89:170-81. https://doi.org/10.1016/j.jmapro.2023.01.070
[38] Kumar D, Kumar P. Microstructural, microhardness and electrical conductivity analysis of AD31T alloy processed by friction stir processing. 2024;xxxx. https://doi.org/10.1108/MMMS-01-2024-0025
[39] Romashkina A, Khovaiko M, Nemov A. Modelling of composite materials with thermoplastic matrices, carbon fibres, and nanoparticles. 2022;49(1):182-92.
[40] Kumar D, Singh S, Angra S. Effect of reinforcements on mechanical and tribological behavior of magnesium-based composites: A review. 2022;50(3):439-58.
[41] Kumar D, Angra S, Singh S. High-temperature dry sliding wear behavior of hybrid aluminum composite reinforced with ceria and graphene nanoparticles. Eng Fail Anal. 2023;151:107426. https://doi.org/10.1016/j.engfailanal.2023.107426
[42] Okafor CE, Okafor EJ, Ikebudu KO. Evaluation of machine learning methods in predicting optimum tensile strength of microwave post-cured composite tailored for weight-sensitiv e applications. Eng Sci Technol Int J. 2022;25:100985. https://doi.org/10.1016/j.jestch.2021.04.004
[43] Mahanta S, Chandrasekaran M, Samanta S, Arunachalam RM. EDM investigation of Al7075 alloy reinforced with B4C and fly ash nanoparticles and parametric optimization for sustainable production. J Braz Soc Mech Sci Eng. 2018;40(5):1-17. https://doi.org/10.1007/s40430-018-1191-8